

APPLICATION OF IMPROVED GABOR DECONVOLUTION ON ZERO-OFFSET VSP DATA USING A NOVEL SMOOTHING METHOD IN LOGARITHMIC SPECTRUM

MOHAMMAD ALI RIAHI

Institute of Geophysics, Department of Solid Earth Physics, University of Tehran, Tehran, Iran. mariahi@ut.ac.ir

(Received February 21, 2020; revised version accepted January 15, 2021)

ABSTRACT

Riahi, M.A., 2021. Application of improved Gabor deconvolution on zero-offset VSP data using a novel smoothing method in logarithmic spectrum. *Journal of Seismic Exploration*, 30: 147-172.

Absorption phenomenon attenuates seismic signal amplitudes, reduces the vertical resolution, and hampers the detection of thin layers. The key objective of this study is the vertical resolution enhancement of zero-offset vertical seismic profile data (ZVSP) by Gabor deconvolution. According to constant Q theory, it is reliable to apply a smoothing along hyperbolic trajectories in the time-frequency domain. In conventional hyperbolic smoothing, an empirical whitening factor is added to stabilize the process. Experiments on real seismic data show that the whitening factor can smear useful information or produce artifacts. To prevent these shortcomings, we apply a logarithmic magnitude spectrum (LMS) hyperbolic smoothing on ZVSP data. As a result, by replacing divisions with subtractions whitening factor is used. Smoothing the Gabor magnitude spectrum of seismic data along hyperbolic paths in the logarithmic spectrum can obtain the magnitude of the attenuation function, eliminate the effect of source wavelet, then, estimate the source wavelet amplitude spectrum. Applying different deconvolution methods on synthetic and real data we show that the performance of the Gabor deconvolution using the LMS is better than that of other methods including Wiener deconvolution and conventional hyperbolic smoothing method.

KEY WORDS: Gabor transform, Gabor deconvolution, smoothing, logarithmic magnitude spectrum, vertical seismic profiling (VSP).

INTRODUCTION

Deconvolution is one of the main stages of processing seismic data to enhance the resolution and detection of multiples. The most commonly used deconvolution method is based on the Wiener filter that was introduced by Treitel and Robinson (1967). A trace can be obtained as a convolution of the seismic wavelet and reflection coefficient (RC) series. In Wiener's method, we can obtain a reflection coefficient (RC) series by using a recorded trace, and this operation is called deconvolution. However, the Wiener method has some conditions, including that the wavelet is a minimum phase and stationary, and RC series is random. In reality, due to the absorption, propagated waveform changes with time, and the so-called propagated wavelet is non-stationary.

For this reason, the use of a non-stationary deconvolution operator is necessary. Gabor deconvolution considers the seismic section as non-stationary data. In this method, the loss of high frequency, amplitude, especially in later times that are attenuated due to absorption and spherical spreading, are approximated and compensated. Different methods of designing deconvolution operators for VSP data have been proposed. Anstey (1976) recommends averaging of the downgoing waves from all levels to design an inverse operator. Lee and Balch (1983) use the downgoing wave from a single level to deconvolve all of the VSP traces. Gaiser et al. (1984) and Hubbard (1979) recommends performing the deconvolution independently at each depth level. Ross and Shah (1987) suggest the level-by-level deconvolution based on the entire downgoing wave train. Sun et al. (2009) suggest the level-by-level deconvolution based on the entire upgoing wavetrain. Gabor deconvolution is a new method based on a non-stationary convolutional model (Margrave et al., 2011). A trace contains a non-stationary seismic wavelet convolved with impulse response (reflection coefficients series), plus noise. The reflection coefficients, series will be calculated if the non-stationary wavelet is obtained. In order to estimate the non-stationary wavelet from a trace, Margrave (1998) proposed the theory of non-stationary filter and a non-stationary deconvolution operator. Then, Margrave and Lamoureaux (2001) developed a non-stationary deconvolution using the Gabor transform. Margrave et al. (2004) proposed a non-stationary deconvolution technique, called hyperbolic smoothing, to eliminate the amplitude equalization effect. Montana and Margrave (2004 and 2005), Montana et al. (2006) used improved Gabor deconvolution performance by phase correction. Margrave et al. (2011) introduced Gabor transform based on a complete set of windows (Erhan and Nowack, 2020) and proposed a Gabor deconvolution algorithm by a spectral smoothing technique. Ahadi and Riahi (2013) applied the Gabor deconvolution method using boxcar smoothing and ordinary hyperbolic smoothing on zero-offset VSP data. Zengbao et al. (2013) applied hyperbolic smoothing as a least-squares inverse problem.

In this paper, a non-stationary deconvolution algorithm based on hyperbolic smoothing in the logarithmic magnitude spectrum is used for vertical seismic profile data. Unlike the conventional method of hyperbolic smoothing, in which each division must necessarily be associated with an experimental whitening factor, the new method of hyperbolic smoothing is in the logarithmic magnitude spectrum, i.e., LMS hyperbolic smoothing. This method mitigates many difficulties in conventional Gabor based methods because the LMS exponential attenuation function transforms into a linear one. At the same time, the effect of a whitening factor is removed by replacing the division by subtraction. Needless to say that the choice of the smoothing method is a key factor that significantly affects the final results. Until now, smoothing along hyperbolic trajectories has been used as a reliable way to obtain wavelet that generated from the effect of the sources and level-lines of attenuation function (Margarve et al., 2011). However, the ordinary hyperbolic smoothing suffers from side effects of the whitening factor added during the iteration process (Sun et al., 2012). On the other hand, a useful method of wavelet estimation is using VSP data, since VSP wavelets travel much less path than similar wavelets generated from surface seismic data (Dong et al., 2002). Therefore VSP data attenuation is less, and the results of applying non-stationary wavelets on VSP data are much closer to the subsurface reality.

THEORY

Gabor transform algorithm

One of the key methods for non-stationary deconvolution is to use the Gabor transform. Gabor proposed the wave propagation in the form of Gaussian wave packets, to focus a signal to a specified time range, and then applies the Fourier transform of the wave packets (Gabor, 1946). In the following, the Gaussian wave packets are described as Gaussian windows. In some papers, the Gabor transform is introduced as a short-time Fourier transform. Repeating the Gaussian function to infinity and then apply a Fourier transform on it, a spectral Fourier spectrum is achieved. By shifting the windows in time and Repeat the above steps, the primary time function is regarded as a function of time, and frequency (seismic signal from the one-dimensional plane is transmitted to a 2D time-frequency plane). Because of the repetitive calculations of continuous Gabor transform, it appears that the use of Gaussian functions in the central discrete times is more appropriate. Discrete Gabor transform is proposed by taking one of the Gaussian functions, features which is (Margrave and Lamoureux, 2001):

$$\sum_{n \in \mathbb{Z}} \Omega(t - n\Delta\tau) = \sum_{n \in \mathbb{Z}} \Omega_n \approx 1 \quad (1)$$

This relationship defines a set of Gaussian windows that the sum of them in every moment is unitary. In eq. (1), Ω_n means the shifted window Ω in the time $n\Delta\tau$. Gaussian functions can be defined as follows (Gabor, 1946):

$$\Omega(t - n\Delta\tau) = \frac{\Delta\tau}{T\sqrt{\pi}} e^{-[t-n\Delta\tau]^2 T^{-2}} \quad (2)$$

In this equation, T is half the width of the Gaussian window, and $\Delta\tau$ is the distance between the Gaussian windows. In order to get $\sum \Omega(t - n\Delta\tau)$ the equation can be written as a convolution with a function:

$$\sum_{n \in \mathbb{Z}} \Omega(t - n\Delta\tau) = (\Omega * C)(t) \quad (3)$$

The function is defined as:

$$C(t) = \sum_n \delta(t - k\Delta\tau) \quad (4)$$

Fourier transform of $C(t)$ and $\Omega(t)$ functions are defined as follows:

$$\hat{\Omega}(f) = e^{-(\pi f T)^2} \Delta\tau \quad (5)$$

$$\hat{C}(f) = \frac{1}{\Delta\tau} \sum_n \delta\left(f - \frac{n}{\Delta\tau}\right) \quad (6)$$

Inserting the relations (5) and (6) in eq. (3), then calculating the inverse Fourier transform, we get:

$$\sum_{n \in \mathbb{Z}} \Omega(t - n\Delta\tau) = 1 + 2 \cos\left(\frac{2\pi t}{\Delta\tau}\right) e^{-\left(\frac{\pi T}{\Delta\tau}\right)^2} \quad (7)$$

The second term of the equation determines the error. Therefore, by increasing $\frac{T}{\Delta\tau}$, the amount of errors is reduced. Figs. (1a) and (1b) display Gaussian windows that the sum of them at every point in the time axis is unitary. The figures were drawn using eq. (7). Near the two sides of the summation curve in Fig. (1b), the graph is bellowing the unit because of the lower total accumulation of Gaussian windows (Margrave and Lamoureux, 2001).

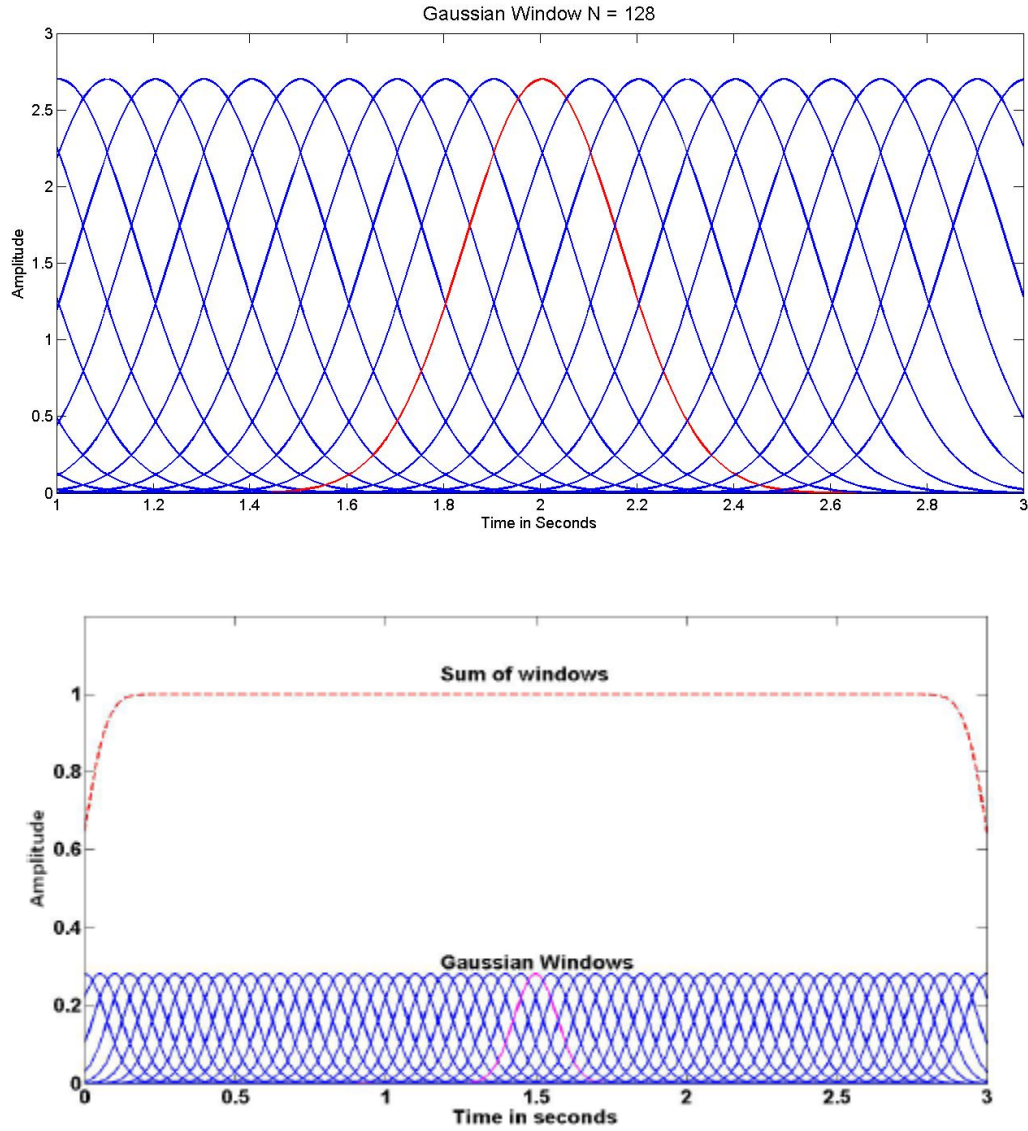


Fig. 1. a) A set of Gaussian windows with the sum-of-windows curve. The window half-width is 0.2 s, and the window increment is 0.1 s. b) On two sides of the summation Curve of Figure, because of the lower total accumulation of Gaussian windows, their summation is just under the unit.

A seismic signal $x(t)$ can be described by Gaussian-like windows as following:

$$\begin{aligned}
 x(t) &= x(t) \sum_{n \in \mathbb{Z}} \Omega(t - n\Delta\tau) = \sum_{n \in \mathbb{Z}} x(t) \Omega(t - n\Delta\tau) \\
 &= \sum_{n \in \mathbb{Z}} x_K(t) \quad .
 \end{aligned} \tag{8}$$

Using the Fourier transform, we get:

$$\begin{aligned}\hat{x}(f) &= \sum_{k \in \mathbb{Z}} x_k(t) e^{-2\pi i f t} dt \\ &= \sum_{k \in \mathbb{Z}} \hat{x}_k(f) \quad .\end{aligned}\tag{9}$$

In eq. (9), \hat{x} is the Fourier transform of x , and $\hat{x}_k(f)$ is the Fourier transform of $x_k(t)$, which means:

$$\hat{x}(f) = \int x_k(t) e^{-2\pi i f t} dt \quad .\tag{10}$$

The original signal can be rewritten by applying an inverse Fourier transform on the eq. (10) as: (Margrave and Lamoureaux, 2001)

$$x(t) = \int \left[\sum_{n \in \mathbb{Z}} x_k(f) \right] e^{2\pi i f t} dt\tag{11}$$

The inverse Gabor transform also was defined as the above equation. It transforms a two-dimensional time-frequency spectrum into a one-dimensional time-domain signal.

Convolutional model for a non-stationary wavelet

Margrave and Lamoureaux (2001) defined a non-stationary wavelet as follows:

$$\hat{w}_\alpha(\tau, \omega) = \hat{w}(\omega) \alpha(\tau, \omega)\tag{12}$$

In the above equation $\hat{w}(\omega)$ is the Fourier transform of source wavelet and attenuation function is defined as follows (Aki and Richards, 1980):

$$\alpha(\tau, \omega) = \exp \left[-\frac{|\omega|}{2Q} \tau + i \frac{\tau}{2Q} H(|\omega|) \right] \quad ,\tag{13}$$

where H denotes the Hilbert transform. The quality factor of rocks is Q , which is the ratio of 2π times the peak power stored in power dissipated per cycle (O'Connell and Budiansky, 1978). The attenuation of seismic energy by the earth and the resulting non-stationary recorded data traces are

fundamental issues in seismic data processing and interpretation. There are two approaches for seismic pulse propagation and dispersion in attenuating media. The first method assumes that Q depends on frequency (Aki and Richards, 1980). The second approach assumes that Q is independent of frequency and is known as the constant- Q model; Q is then used to calculate the pulse broadening and dispersion. Therefore, a non-stationary synthetic trace can be constructed by a non-stationary convolution of the Q operator and the reflectivity, and then a stationary convolution with the wavelet. Here, we assume that Q is independent of frequency, which is called the constant- Q model (Kjartansson, 1979). Margrave (1998) proposed a non-stationary filtering theory and a non-stationary convolution. Applicability of non-stationary deconvolution largely depends on the accuracy of non-stationary wavelet estimation. A non-stationary seismic trace can be defined as follows (Margrave, 1998):

$$\hat{x}(\omega) = \int \hat{w}_\alpha(\tau, \omega) r(\tau) e^{-i\omega\tau} d\tau \quad (14)$$

inserting the non-stationary wavelet equation into eq. (14) we get:

$$\hat{x}(\omega) = \hat{w}(\omega) \int \alpha(\tau, \omega) r(\tau) e^{-i\omega\tau} d\tau \quad , \quad (15)$$

$\hat{x}(\omega)$ is a Fourier spectrum of trace, $\hat{w}(\omega)$ is a Fourier spectrum of source wavelet, r is reflection coefficients, series, and is a time and frequency-dependent attenuation function defined in eq. (13).

The non-stationary seismic trace in the time domain can be given by an inverse Fourier transform of eq. (15), as follows:

$$x(t) = \iint \hat{w}(f) \alpha(u, f) r(u) e^{2\pi i f(t-u)} df du \quad . \quad (16)$$

Eq. (16) shows the convolution between the non-stationary wavelet and a reflection coefficients series.

The Gabor spectrum of a seismic trace is expressed as (Margrave and Lamoureaux, 2001):

$$G[x(\tau, f)] \approx (f) \alpha_0(\tau, f) G[r(\tau, f)] \quad , \quad (17)$$

where the $G[r(\tau, f)]$ is the Gabor spectrum of reflectivity. The important point is that there is no need to calculate the phase; by estimation of $|\hat{w}(f)| |\alpha_0(\tau, f)|$ we can consider a minimum-phase function. Now we assume that $|G[x(\tau, f)]|$ is a function that shifts rapidly in both time and frequency domains. Also, we assume that $|\hat{w}(f)|$ is independent of τ and is smooth in f , while $\alpha_0(\tau, f)$ is exponentially attenuated in both the time and frequency. Assumptions that we consider for $|G[r(\tau, f)]|$ is similar to a

random series of reflection coefficients, which is considered in the theory of stationary deconvolution. The assumed Gaussian window is effective where the signal's components have dissimilar frequencies and amplitudes so that the selected window is shorter in time, the frequency will be smoother and vice versa (Cattani and Rushchitsky, 2007) We estimate the attenuated wavelet in the Gabor domain $|\hat{w}(f)||\alpha_Q(\tau, f)|$ by smoothing $|G[x(\tau, f)]|$. This will be carried out by convolving it with a hyperbolic function in the time-frequency domain. The method evaluated in this paper is an improvement to the other smoothing methods.

By smoothing, we can eliminate the effect of the reflectivity from a seismic trace (Margrave et al., 2002; Ross and Shah, 1987).

Hyperbolic smoothing

Hyperbolic smoothing, tries to estimate the attenuation function and the Gabor spectrum of source wavelet separately. Suppose that $\alpha(t, f)$ is the attenuation function or Q-constant operator, where t is time and f is frequency. We have,

$$\alpha(t, f) = e^{\frac{-\pi t f}{Q} - iH\left(\frac{-\pi t f}{Q}\right)} \quad (18)$$

As eq. (18) shows, in a constant Q model the attenuation contours are determined by $tf = \text{Constant}$, and appear as a family of hyperbolas. Based on this analysis, it is reasonable to divide the entire time-frequency plane into a number of hyperbolic strips, average over each strip, and take these average values as a measurement of the amplitude loss caused by the attenuation. At first, the attenuation surface can be roughly approximated by filling these strips with their respective average values (or by interpolation). Let $I_n(t, f)$ be the indicator function for the n -th hyperbolic strip, in other words, I_n is zero everywhere except where the points inside the n -th strip is unity. This process can be shown in two equations (Sun et al., 2012),

$$a_n = \text{mean}_{t,f}(|G[x(\tau, f)]|I_n(t, f)) \quad , \quad (19)$$

$$|\alpha(\tau, f)|_{est} = \sum_{n=1}^N a_n I_n(t, f) \quad , \quad (20)$$

where N is the total number of hyperbolic strips. Given the $|\alpha(\tau, f)|_{est}$, the source signature $\hat{W}(f)$ can be obtained by averaging the $\frac{|G[x(\tau, f)]|}{|\alpha(\tau, f)|_{est}}$ over all time samples and then running smoothing in the frequency direction with a

suitable convolutional smoother $b(f)$, which is a 2D boxcar (Margrave, 2011),

$$|\widehat{W}(f)|_{est} = b(f) * \mathit{mean}_t \left(\frac{|G[x(\tau, f)]|}{|\alpha(\tau, f)|_{est} + \varepsilon A_{max}} \right) , \quad (21)$$

where $*$ denotes the convolution operator, ε is an extra whitening factor to prevent any division by 0, and A_{max} is the maximum value of dividends. Because of the existence of source signature, the first estimation of $|\alpha(\tau, f)|$ is always higher than the actual value, which will cause an underestimated source in eq. (22). If we remove $|\widehat{W}(f)|_{est}$ from $|G[x(\tau, f)]|$, and repeat the hyperbolic smoothing, a more authentic attenuation function will be obtained. Therefore, an iterative process is favorable in eliminating the residual source effect from the estimation of $|\alpha(\tau, f)|$ (Sun et al., 2012).

These whitening factor during the iteration are the primary concern of our study; it is found that these factors will also influence the ultimate results. This leaves room for further improvement in hyperbolic smoothing.

LMS Hyperbolic smoothing

In the logarithmic magnitude spectrum (LMS), the attenuation surfaces still track along hyperbolic trajectories, and LMS hyperbolic smoothing means the hyperbolic smoothing in this spectrum. There are two major advantages over the hyperbolic smoothing method in the normal spectrum. The exponential relationship of amplitude loss versus the time and frequency is transformed into a linear relationship in LMS, simplifying many problems. More importantly, divisions in the ordinary magnitude spectrum will be converted into subtractions in LMS, which is useful in avoiding the artifacts caused by the whitening factor and reducing human intervention (Sun et al., 2012).

As the solid black line is shown in Fig. 2, the attenuation function in LMS is transformed into linear form with respect to tf

$$L_\alpha(t, f) = \frac{-\pi}{Q} tf \quad , \quad (22)$$

where, L_α stands for the logarithm operation on $|\alpha(\tau, f)|$. Furthermore, the actual logarithmic magnitude spectrum could be formulated as an addition of 3 terms.

$$L_{|G[x]|}(t, f) = \frac{-\pi}{Q} tf + L_{\hat{w}}(f) + L_{G[r]}(t, f) \quad (23)$$

It is evident that this linear relationship's gradient is closely related to Q , while the intercept is caused by source and reflectivity.

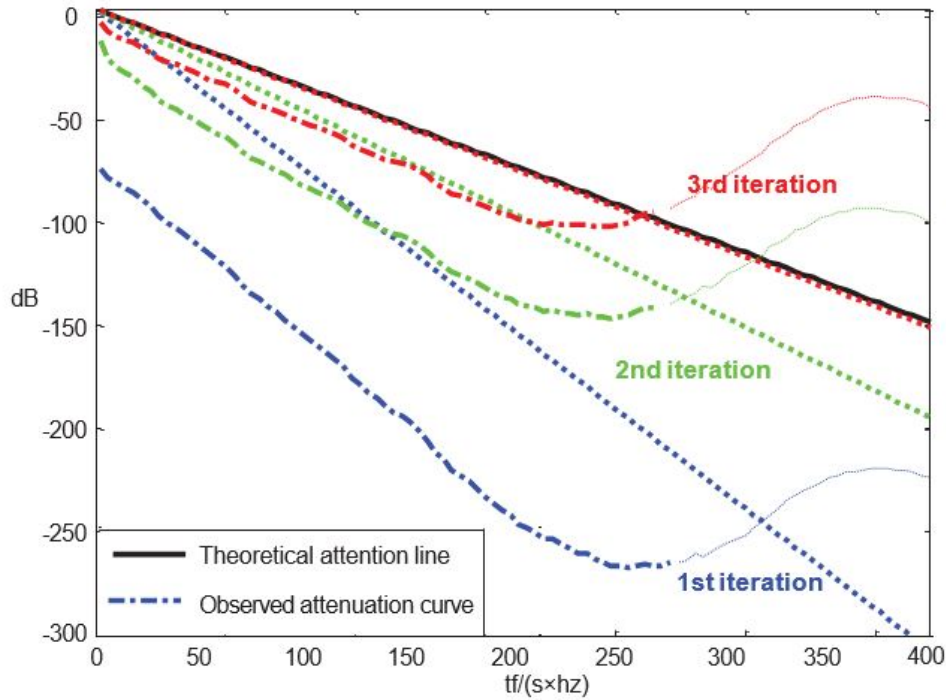


Fig. 2. Iteration process of seeking the optimum Q (Sun et al., 2012).

After dividing the LMS into numbers of hyperbolic strips and then cross-plotting the magnitude average with the center position of each strip, we will get an 'attenuation curve' (the dotted dash lines in Fig. 1). Because the curve's tail is collected at larger tf , an area with insufficient samples for creating a convincing statistical character, it is often cut off before seeking an optimum linear fit. Dropping the intercept term, the attenuation function could be obtained by utilizing the Q extracted from optimum linear fit's gradient. Similarly, the Q estimation should be set in an iteration process. As shown in Fig. 2, an attenuation function with satisfying accuracy is generated only after several iterations. And the source $L_{\hat{w}}$ could be acquired after subtracting the attenuation from $L_{|G[x]|}$, and then averaging over all time and smoothing slightly in frequency. Actually, the mathematical logic behind the eqs. (19) to (22) still makes sense in LMS hyperbolic smoothing, except that division should be replaced by subtraction. This is useful when it comes to experimental seismic data, for that the assumption of a constant Q is rather impractical for the whole seismic section (Sun et al., 2012).

Deconvolution algorithm in Gabor domain

The next step is to estimate the Gabor spectrum of the reflectivity series. For this purpose, the Gabor spectrum of the trace should be divided by the Gabor spectrum of the wavelet:

$$G[r(\tau, f)] = \frac{G[x(\tau, f)]}{|G[x(\tau, f)]|_{smooth} e^{i\varphi(\tau, f)} e^{iH[|\hat{w}_\alpha(\tau, f)|]_{est}}} \quad (24)$$

This division is called deconvolution, and because it has been done in the Gabor domain, it is called deconvolution in the Gabor domain or Gabor deconvolution. By applying the inverse Gabor transform to the Gabor spectrum of the reflectivity, the reflectivity in the time domain is obtained.

In what follows, the process is applied to synthetic and experimental 1 zero-offset VSP data.

Gabor deconvolution of synthetic VSP data

The designed synthetic model consists of 10 layers, where each layer thickness and velocity are shown in Table 1. In this model, receivers spacing is 50 m, and Q is set to be 40. Fig. 3, top and bottom, shows synthetic zero-offset VSP data without and with 10% random noise, respectively. These sections are composed of downgoing and upgoing waves. Upgoing waves are reflections received from deep layers, and downgoing waves are direct arrivals.

Table 1. Shows the velocity and thickness of each layer.

| Layers | Thickness (m) | Velocity (m/s) |
|--------|---------------|----------------|
| 1 | 160 | 800 |
| 2 | 150 | 1300 |
| 3 | 130 | 2100 |
| 4 | 200 | 1700 |
| 5 | 190 | 2000 |
| 6 | 110 | 2200 |
| 7 | 185 | 2400 |
| 8 | 220 | 2100 |
| 9 | 85 | 1900 |
| 10 | 130 | 2550 |

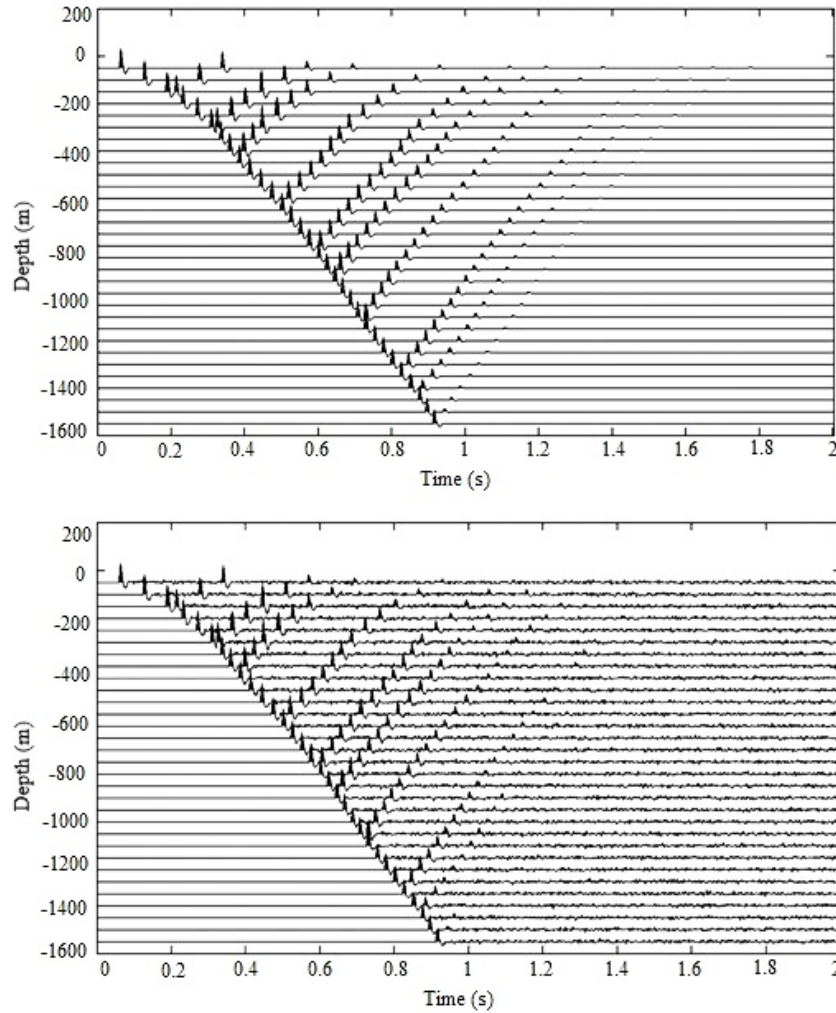


Fig. 3. Zero-offset VSP data designed according to Table 1. Data without noise (top) and data with 10% random noise (bottom).

In VSP data processing, to apply the deconvolution operator, it is necessary to separate the upgoing wavefield from the downgoing wavefields. In this study, for the separation of these two wavefields, a median filter (Hardage, 1983) is used. Fig. 4 shows the flattened upgoing waves in both the clean and noisy data sets. From Fig. 4, in particular, it is seen that the reflections received from the 10-th layer are affected by a severe amplitude attenuation. These reflections are hardly detectable in the noisy data. Some amounts of amplitude attenuation are also seen in the reflections received from the eighth and ninth layers. These reflections are marked by ellipses in both data sets in Fig. 4. After the aforementioned step, the VSP data are ready for applying the deconvolution operator.

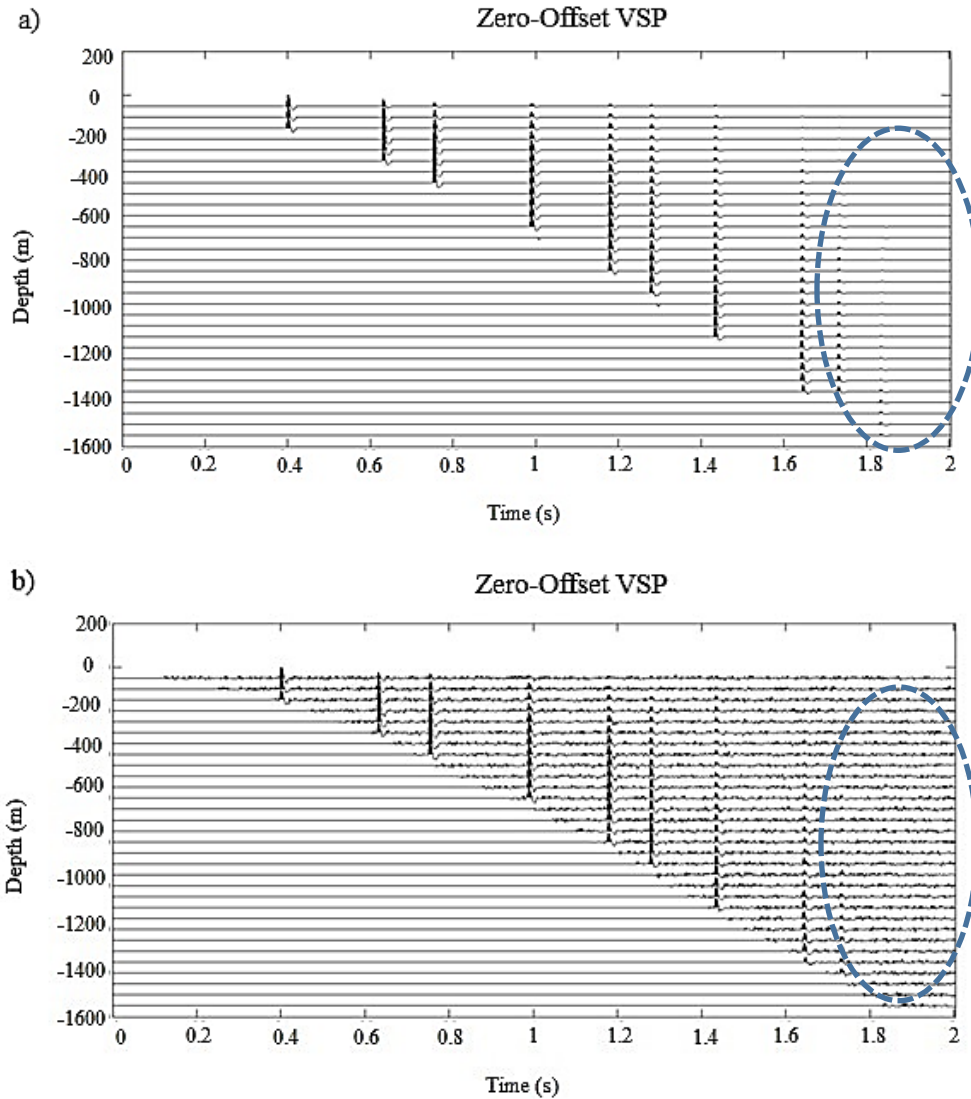


Fig. 4. Flattened and separated upgoing waves in both data sets without noise (top) and with 10% random noise (bottom).

The deconvolution operator is designed by using the downgoing waves in the VSP data. The required seismic wavelet for deconvolution of the upgoing data is also estimated using the same waves. It should be noted that the improved Gabor deconvolution is applied separately to each trace of the seismic section. Wavelet estimation is one of the most important stages of a deconvolution. To evaluate the precision of the wavelet estimation by LMS hyperbolic smoothing, the seismic wavelet is selected from downgoing wavefields. Next, based on the method proposed by Gaiser et al. (1984), the deconvolution operator is used independently on each layer. The results of using proper estimation of the upgoing waves by the proposed LMS hyperbolic smoothing are shown in Fig. 5.

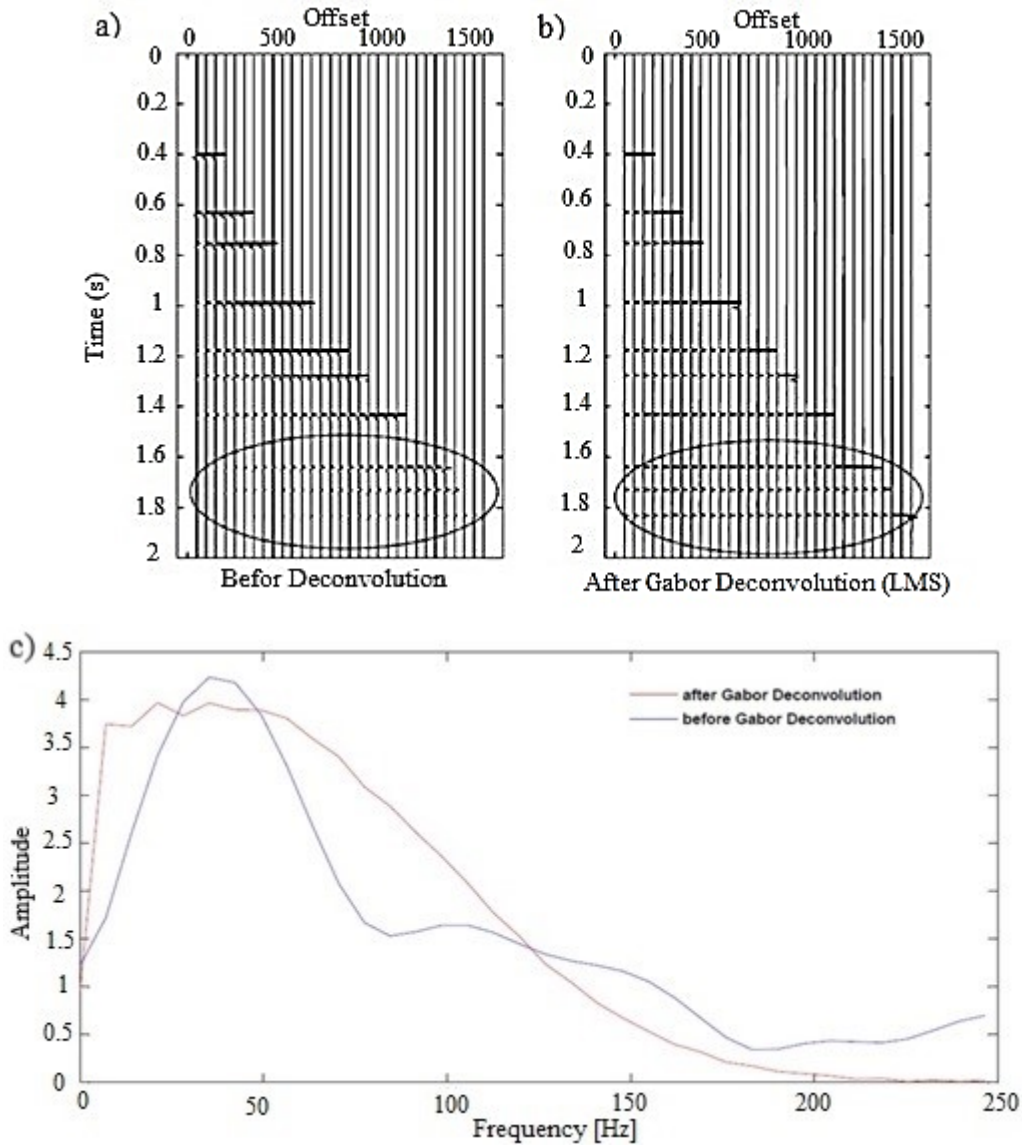


Fig. 5. Shows the results before (panel a) and after Gabor deconvolution with LMS approach on upcoming reflections (panel b). Note that for both cases, the final results show the improvements in amplitude (attenuation case). c) A comparison between the amplitude spectrum before (blue curve) and after applying improved Gabor deconvolution (red curve).

In the above figures, the severe attenuation in amplitude is obvious in reflections shown within the ellipse in the top left panel before applying LMS Gabor deconvolution. While considerable enhancement in the amplitude of the reflections shown within the ellipse in the top right panel after applying LMS Gabor deconvolution. This enhancement is due to the proper estimation of the wavelet by the proposed LMS hyperbolic smoothing.

For the noise-contaminated data the results are shown in Fig. 6. In this figure, the severe attenuation in amplitude is obvious in reflections shown within the ellipse in the bottom left panel before applying LMS Gabor deconvolution. While considerable enhancement in the amplitude of the reflections shown within the ellipse in the bottom right panel after applying LMS Gabor deconvolution. This enhancement is due to the proper estimation of the wavelet by the proposed LMS hyperbolic smoothing. A comparison between amplitude spectrum before (blue line) and after applying improved Gabor deconvolution (red line).

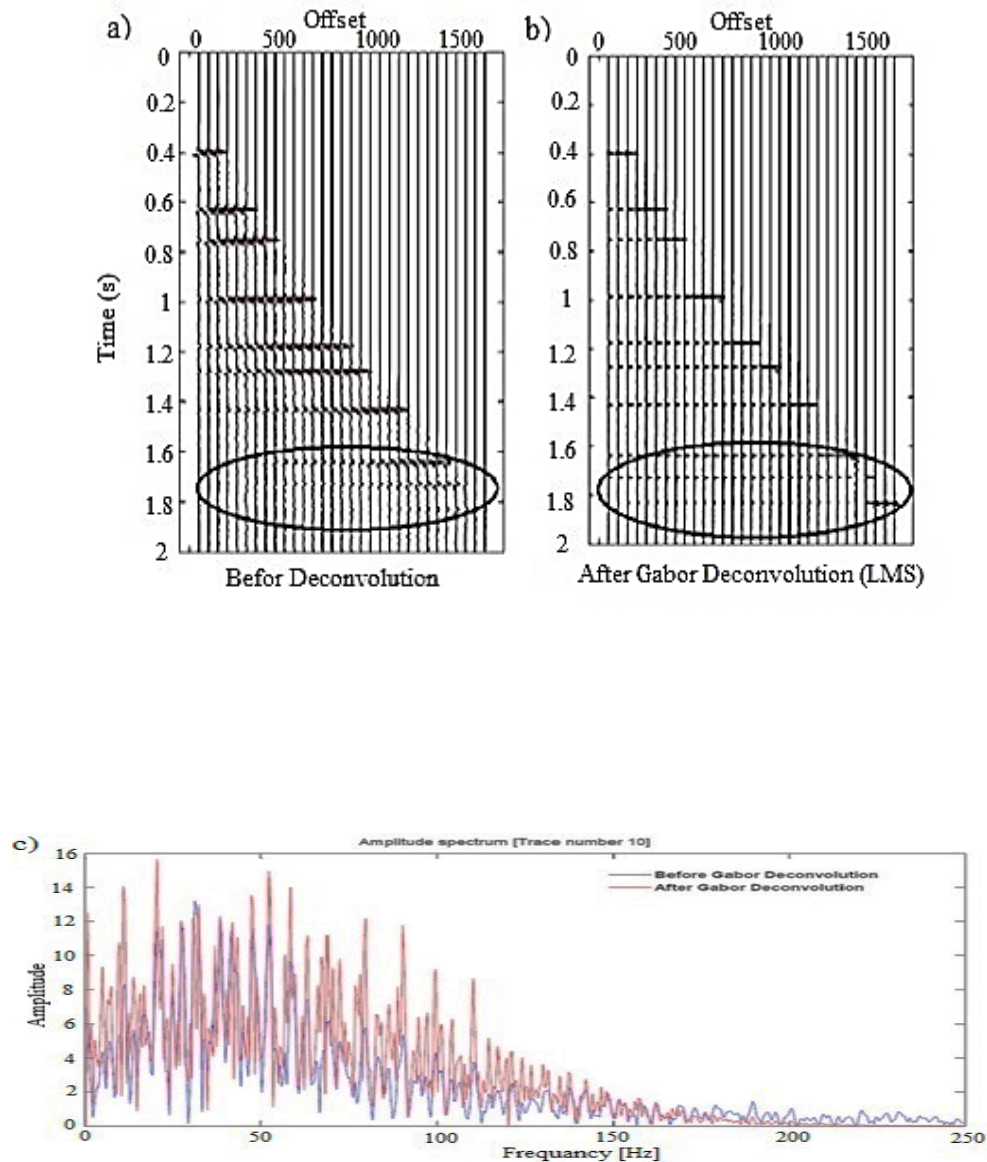


Fig. 6. Zero-offset VSP data of Fig. 4 after applying improved Gabor deconvolution designed from downgoing waves on to data without noise (a) and to data with 10% random noise (b). c) A comparison between the amplitude spectrum before (blue line) and after applying improved Gabor deconvolution (red line).

To have a better comparison of the proposed method with the conventional Wiener deconvolution. The Wiener deconvolution operator is designed by using the downgoing VSP waves and applied to the upgoing waves. The Wiener deconvolution with ordinary hyperbolic smoothing applied to the same model used by Ahadi and Riahi (2013). As shown in Fig. 7, the results obtained after applying the Wiener deconvolution, the reflections marked with an arrow are not enhanced. In addition, a series of artifacts that may cause confusion appears parallel to the primary reflections marked within the ellipses in Fig. 7.

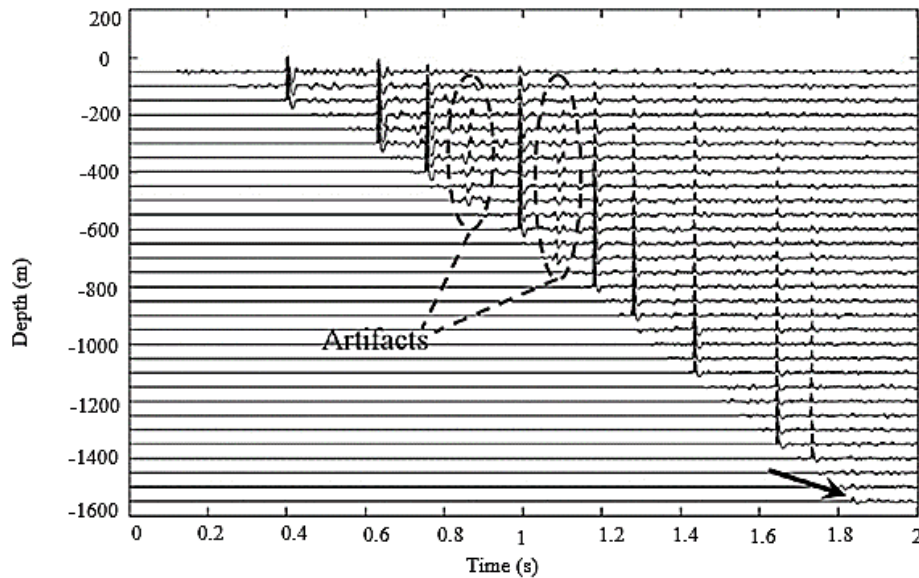


Fig. 7. Zero-offset VSP data using conventional hyperbolic smoothing, an empirical whitening factor is added to stabilize the process. The Wiener deconvolution is applied to data with a 10% random noise. Artifacts are visible in the ellipses. Using the conventional hyperbolic smoothing, the whitening factor smeared useful information and produced artifacts.

The results presented in Fig. 8 clearly show that the LMS Gabor deconvolution has a greater ability to restore attenuated reflections than the Wiener deconvolution. Despite a sharp attenuation in signal amplitudes before deconvolution in the deep reflections shown within an ellipse (bottom left panel), using improved Gabor deconvolution shows a noticeable amplitude enhancement in the deep reflections (bottom right panel). Namely that, using the Gabor deconvolution has increased the amplitude of reflections received from deeper layers, whereas reflections amplitudes are not well reconstructed after applying the Wiener deconvolution (Fig. 7).

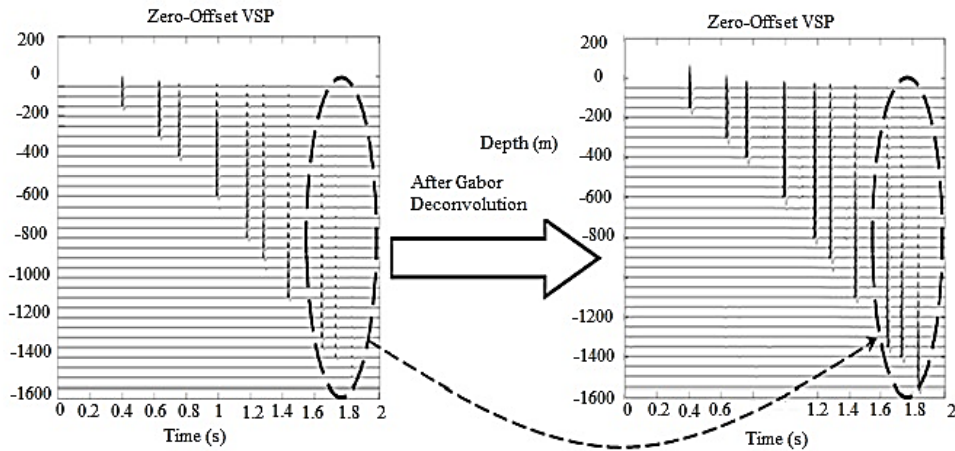


Fig. 8. Zero-offset VSP data of before (left panel) and after (right) using conventional Gabor deconvolution designed from downgoing waves on to data without noise. The attenuated reflection amplitudes shown within left ellipse are noticeably enhanced within the right ellipse after using Gabor deconvolution.

To examine the stability of the LMS Gabor deconvolution via the presence of random noise, 10% random noise added to the Zero-offset VSP data. Figs. 9a and 9b, show the results of noisy data before (left panel) and after (right) using the LMS Gabor deconvolution. The attenuated reflection amplitudes are shown within the left ellipse are noticeably enhanced in the right ellipse after using the LMS Gabor deconvolution. Indicating that, by using logarithmic magnitude spectrum (LMS) hyperbolic smoothing is stable via the presence of random noise and illuminates useful information, and eliminates artifacts.

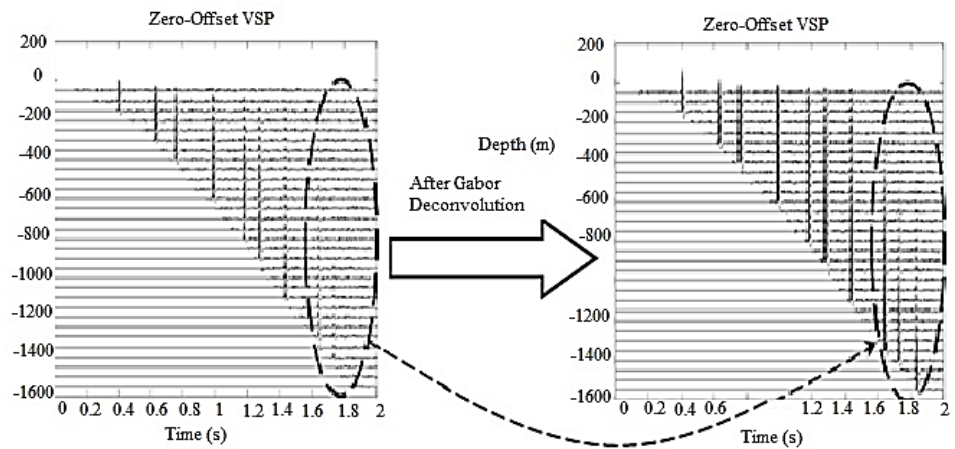


Fig. 9. Zero-offset VSP data before (left panel) and after (right) using the LMS Gabor deconvolution designed from up-going waves on to data with a 10% random noise. The attenuated reflection amplitudes is shown within the left ellipse are noticeably enhanced in the right ellipse after using Gabor deconvolution. Using logarithmic magnitude spectrum (LMS) hyperbolic smoothing illuminates useful information and eliminates artifacts.

The deconvolution operator was designed by separating downgoing wavefields from the upgoing wavefield in the aforementioned data, and the processes go on with designing a deconvolution operator with downgoing wavefield and then applying to the upgoing wavefield. LMS hyperbolic smoothing is used to estimate non-stationary wavelets. Fig. 10a shows the Gabor transform of traces in LMS domain with 20 hyperbolae of $tf = \text{constant}$, smoothing through these strips we can obtain an estimation of non-stationary wavelet. Fig. 10b shows the Gabor spectrum of reflectivity resulted in improved Gabor deconvolution.

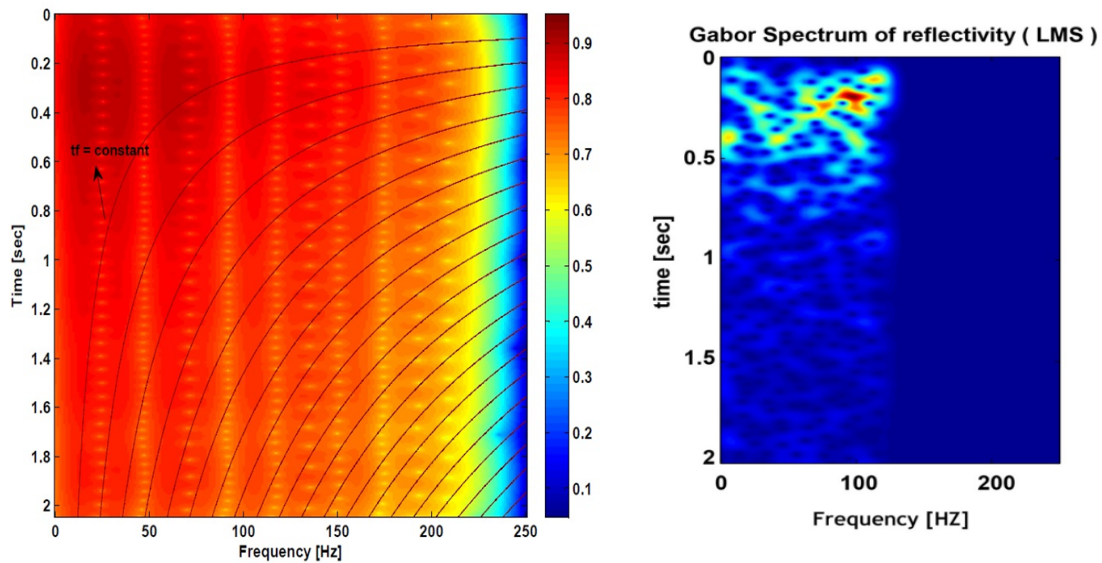


Fig. 10. The Gabor transform of traces in the logarithmic magnitude spectrum with 20 hyperbolae of $tf = \text{constant}$ (Left) and Gabor spectrum of reflectivity resulted by applying Gabor deconvolution with LMS approach (right).

Gabor deconvolution of experimental VSP data

Above, deconvolution results from synthetic data were studied in the Gabor domain. In this step, the Gabor deconvolution is applied to an experimental zero-offset VSP data set. The data are from one of the southern Iranian oil fields. It is worth mentioning that the processing steps in the experimental data are performed using the MATLAB software (the Matlab script is included in the Appendix). Fig. 11 represents the experimental VSP data. This data contains 243 traces, and geophone interval are 15 m, the sampling interval is 2 ms. The acquisition depth is from 712 to 4235 m, we have chosen 80 traces from 1755 to 2954 m and apply improved Gabor deconvolution on them. Fig. 12 shows the experimental data after applying AGC, the upgoing, and downgoing waves are observable.

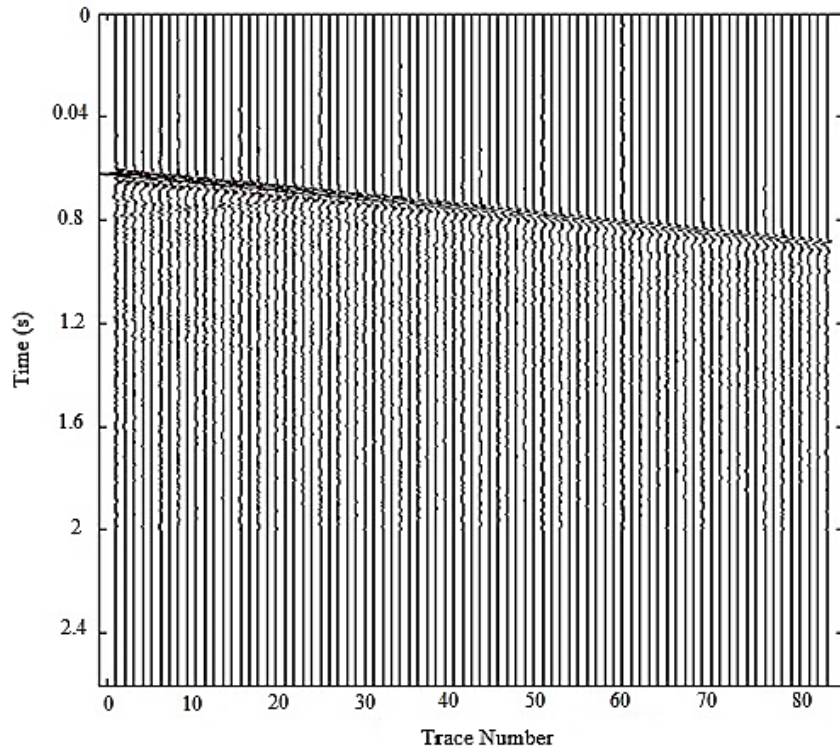


Fig. 11. Zero-offset VSP experimental data.

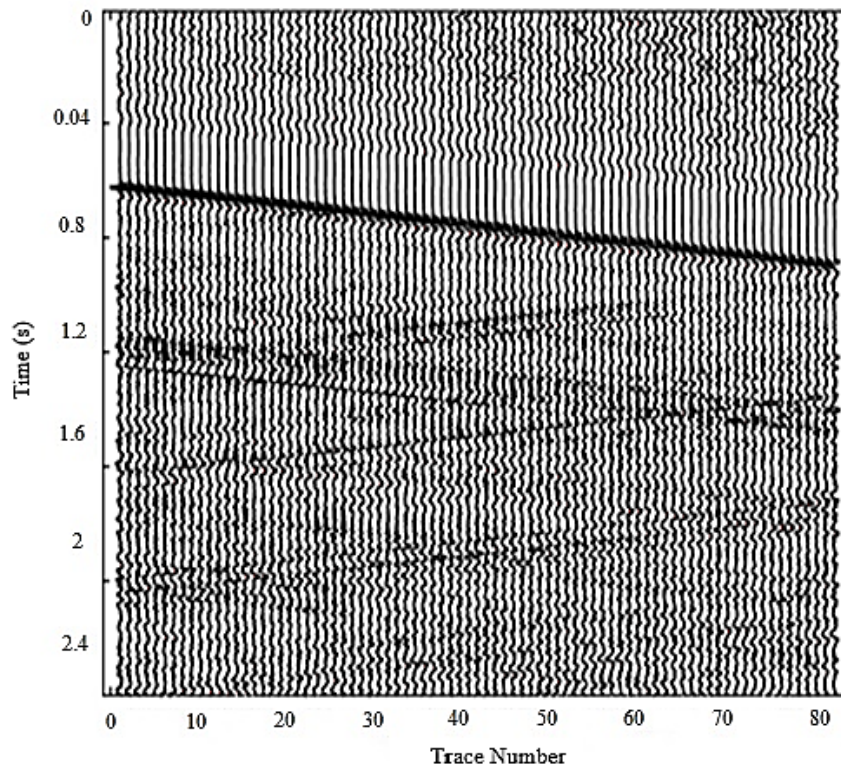


Fig. 12. Zero-offset VSP experimental data after applying AGC.

After flattening the upgoing waves and applying median filters (to separate upgoing and downgoing waves), the experimental data are ready for the application of the deconvolution operator. Fig. 13 shows the experimental data after performing these steps. The deconvolution operator of the Gabor domain is designed based on the downgoing waves and applied to the upgoing waves. The results can be seen in Fig. 14 where reconstruction of the reflections is shown by the yellow ovals in this figure.

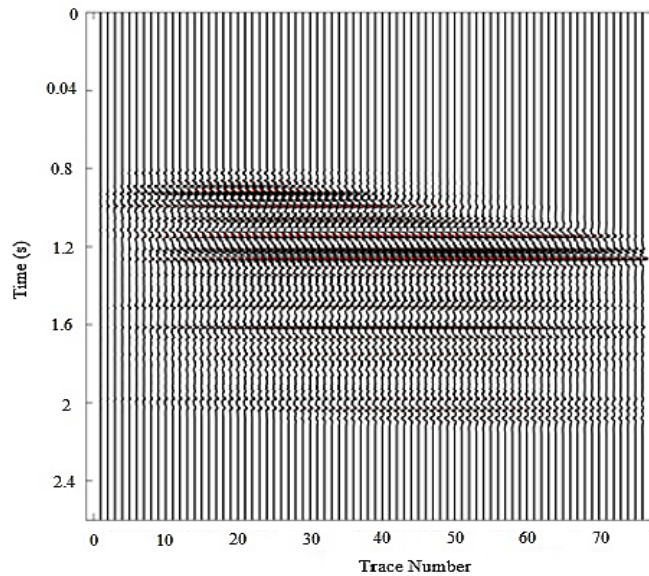


Fig. 13. Flattened and separated upgoing waves before applying Gabor deconvolution.

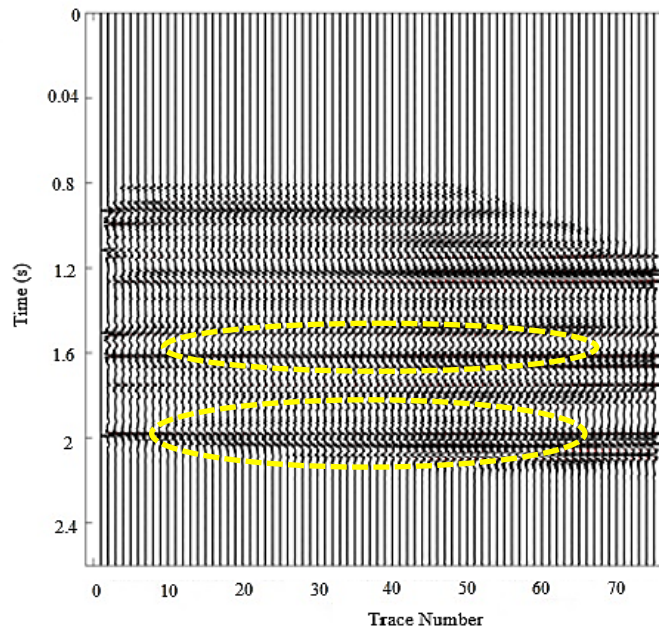


Fig. 14. Upgoing waves after applying the improved Gabor deconvolution. A noticeable improvement is obvious on reflectors at 1.6 and 2 seconds, respectively.

In order to clarify the results, a comparison has been made between three experimental recorded seismographs in three different depths before and after applying Gabor deconvolution. These three seismographs were selected from depths of 100, 750, and 1300 m, which are shown in Fig. 15, respectively. As is noticeable, these three traces are improved considerably after applying the improved Gabor deconvolution.

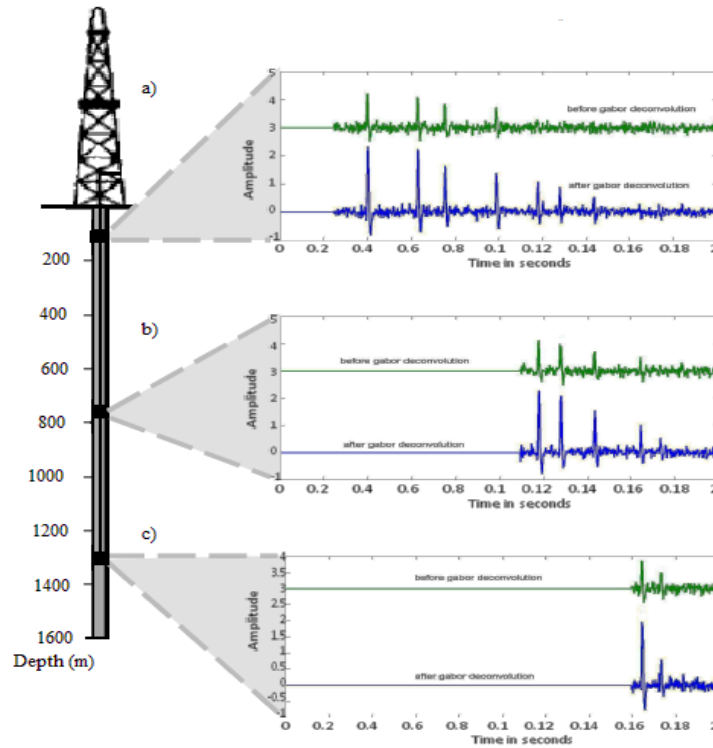


Fig. 15. shows three seismographs selected from depths of 100, 750, and 1300 meters, which are resulted before (green) and after (blue) applying improved Gabor deconvolution, respectively. As is noticeable, these three traces are improved considerably after applying the Gabor deconvolution.

CONCLUSION

Gabor deconvolution includes an amplifier function that can affect the amplitude of the estimated nonstationary wavelets. Application of our improved Gabor deconvolution with LMS hyperbolic smoothing on two synthetic VSP data sets (with and without random noise) showed a higher resolution and improved reconstruction of wavelets, compared with the Wiener and conventional Gabor deconvolution operators. Using the improved Gabor deconvolution operator on real VSP data we observed an increase in quality and resolution and an improvement in the reconstruction of different reflections. Our method also makes data processing faster. In the presented Gabor deconvolution, it is not necessary to separately eliminate the attenuation effect, as is in the conventional method. In LMS, the

exponential equation transforms into a linear form, therefore it avoids a whitening factor that is conventionally selected by a user. Our results demonstrate that our improved Gabor deconvolution can successfully estimate nonstationary wavelets from zero-offset VSP data. It improves the quality of VSP data without considerable sensitivity to random noise. This is shown by comparing our improved Gabor deconvolution operator with Wiener and conventional Gabor deconvolution operators.

ACKNOWLEDGMENT

I would like to acknowledge the Research Council of the University of Tehran. For the purpose of the application of this method of VSP data, the author has benefited from the CREWES site for which they appreciate the authorities of this site. This research did not receive any specific grant from funding agencies in the public, commercial, or not-for-profit sectors.

REFERENCES

- Ahadi, A. and Riahi, M.A., 2013. Application of Gabor deconvolution to zero-offset VSP data. *Geophysics*, 78(2): D85-D91. doi:10.1190/GEO2011-0319.1
- Aki, K. and Richards, P.G., 1980. *Quantitative Seismology: Theory and Methods*. W.H. Freeman & Co., San Francisco.
- Anstey, N., 1976. Seismic delineation of oil and gas reservoirs using borehole geophones. Canadian Patents 1,106,957 and 1,114, 937.
- Cattani, C. and Rushchitsky, J., 2007. *Wavelet and Wave Analysis as Applied to Materials with Micro or Nanostructure*. World Scientific Publishing Company, Singapore. doi: 10.1142/9789812709769.
- Chen, Z., Wang, Y., Chen, X. and Li, J., 2013. High-resolution seismic processing by Gabor deconvolution. *J. Geophys. Engineer.*, 10(6): 065002. doi: 10.1088/1742-2132/10/6/065002.
- Dong, L., Margrave, G.F. and Hall, K.W., 2002. Comparison of wavelet estimates from VSP and surface data. CREWES Research Report, 14: 1-6.
- Erhan, E. and Nowack, R.L., 2020. Application of non-stationary iterative time-domain deconvolution. *Stud. Geophys. Geod.*, 64: 76-99. doi.org/10.1007/s11200-019-1165-z
- Gabor, D., 1946. Theory of communication. *IEEE Transact. Informat. Theory*, 93: 429-457.
- Gaiser, J.E., Disiena, J.P. and Fix, J.E., 1984. Vertical seismic profiles: Fundamentals of the downgoing wavefield and applications that improve CDP data interpretation. In: Toksöz and Stewart (Eds.), *Vertical Seismic Profiling, Part B: Advanced Concepts*. Geophysical Press, Amsterdam: 87-112.
- Hardage, B.A., 1983. *Vertical Seismic Profiling, Part A: Principles*. Geophysical Press, Amsterdam.
- Hubbard, T.P., 1979. Deconvolution of surface recorded data using vertical seismic profiles. *Expanded Abstr.*, 49th Ann. Internat. SEG Mtg., New Orleans.
- Kjartansson, E., 1979. Constant Q-wave propagation and attenuation. *J. Geophys. Res.*, 84: 4737-4748. doi: 10.1029/JB084iB09p04737.

- Lee, M.W. and Balch, A.H., 1983. Computer processing of vertical seismic profile data. *Geophysics*, 48: 272-287. doi: 10.1190/1.1441467.
- Margrave, G.F. Henley, D.C., Lamoureux, M.P., Iliescu, V. and Grossman, J.P., 2002. An update on Gabor deconvolution. *CREWES Res. Rep.*, 14.
- Margrave, G.F. and Lamoureux, M.P., 2001. Gabor deconvolution. *CREWES Res. Rep.*, 13.
- Margrave, G.F., Lamoureux, M.P. and Henley, D.C., 2011. Gabor deconvolution: Estimating reflectivity by nonstationary deconvolution of seismic data. *Geophysics*, 76(3): W15-W30. doi: 10.1190/1.3560167.
- Montana, C.A. and Margrave, G.F., 2005. Hilbert transform, Gabor deconvolution and phase corrections. *CREWES Res. Rep.*, 17.
- Montana, C.A. and Margrave, G.F., 2004. Phase correction in Gabor deconvolution. *CREWES Res. Rep.*, 16.
- Montana, C.A., Margrave, G.F. and Henley, D., 2006. Surface-consistent Gabor deconvolution. *CREWES Res. Rep.*, 18.
- O'Connell, R.J. and Budiansky, B., 1978. Measures of dissipation in viscoelastic media. *Geophys. Res. Lett.*, 5: 5-8. doi: 10.1029/GL005i001p00005.
- Ross, W.S. and Shah, P.M., 1987. Vertical seismic profile reflectivity: Ups over downs. *Geophysics*, 52: 1149-1154. doi: 10.1190/1.1442379.
- Sun, X.E., Ling, Y., Gao, J., Lin, J. and Sun, D., 2009. A deconvolution approach using statistical upgoing waves of zero offset VSP. *Extended Abstr., 71st EAGE Conf., Amsterdam.*
- Sun, X., Sun, S.Z, Peng, T. and Wu, S., 2012. Gabor deconvolution: Hyperbolic smoothing in logarithmic magnitude spectrum. *Expandd Abstr., 82nd Ann. Internat. SEG Mtg., Las Vegas.*

APPENDIX

```
%Gabor Transform
function [ tfs,tout,fout,tnorm ] =
Gabor_transform2(trace,t,twindow,tincrease );

    taper=200;
    normalize=1;
    power=1;

taper=taper*twindow/max(t);

tmin=t(1);
t=t-tmin;

%row vectors
[m,n]=size(trace);
if(n==1) trace=trace.'; end
[m,n]=size(t);
if(n==1) t=t'; end
dt=t(2)-t(1);

%taper trace
trace=trace.*mwhalf(length(trace),taper)';

%power trace
trace=padpow2(trace);
```

```

t=(0:length(trace)-1)*(t(2)-t(1));
%number of windows
tmax=t(end);
nwin=tmax/tincrease+1;
nwin=round(nwin);
tinc=tmax/(nwin-1);
tout=(0:nwin-1)*tinc;
tnorm=zeros(size(t));
itn=zeros(1,nwin);

for k=1:nwin
    %Gaussian
    tnot=(k-1)*tinc;
    itn(k)=round((tnot-t(1))/dt)+1;
    gwin=exp(-(t-tnot)/twindow).^2/(sqrt(pi)*twindow/tincrease);
    tnorm=tnorm+gwin;

    if(k==1)
        [tmp,fout]=fftrl(gwin.*trace,t);
        tfs=zeros(nwin,length(tmp));
        tfs(k,:)=tmp;
    elseif(k<nwin)
        tfs(k,:)=fftrl(gwin.*trace,t);
    else
        tfs(k,:)=fftrl(gwin.*trace,t);
    end
end
end
function [spechyp,smooth,tf] = hyperbolic_smoothing(tfs,t,f,n)

%n=levels in Smoothing

nt=length(t);
nf=length(f);

if(n>nf)
    n=nf;
end

if(nargin<4)
    n=nf;
end

tfmax=t(end)*f(end);
deltf=tfmax/n;

tf=t(:)*(f(:)');

smooth=zeros(1,n+1);
fold=smooth;
tflevels=linspace(0,tfmax,n+1);
for k=1:nf
    for kk=1:nt
        tf1=tf(kk,k);
        klevel=floor(tf1/deltf)+1;
        smooth(klevel)=smooth(klevel)+tfs(kk,k);
    end
end

```

```

        fold(klevel)=fold(klevel)+1;
    end
end
%Hyperbolic Smoothing
smooth=smooth./fold;

spechyp=zeros(size(tfs));
for k=1:nt
    for kk=1:nf
        iuse1=floor(tf(k, kk)/deltf)+1;
        iuse2=ceil(tf(k, kk)/deltf)+1;
        if(iuse2==iuse1)
            spechyp(k, kk)=smooth(iuse1);
        else
            spechyp(k, kk)=smooth(iuse1)+(smooth(iuse2)-
smooth(iuse1))*...
                (tf(k, kk)-tflevels(iuse1))/(tflevels(iuse2)-
tflevels(iuse1));
        end
    end
end
function [ trout,spectrum ] =
gabordeconvolution(trace,t,twindow,tincrease,tsmoothing,fsmoothing,s
tab,phase,ioperator)

% ioperator      1 operator with analysis windowing
%               2 operator with synthesis windowing
%
% stab          stability constant
%
% phase         0 for zero phase, 1 for minimum phase

[ tfs,tout,fout ] = Gabor_transform2( trace,t,twindow,tincrease );

tmp=max(tfs,[],2);%Find the maximum of each spectrum
amax=abs(min(tmp));

dt=tout(2)-tout(1);
df=fout(2)-fout(1);
nt=round(tsmoothing/dt)+1;
nf=round(fsmoothing/df)+1;

if(tsmoothing<max(t))
    % smooth with boxcar smoothing
    spectrum=conv2(abs(tfs)+stab*amax,ones(nt,nf),'same');
else
    %hyperbolic smoothing
    spechyp=hyperbolic_smoothing(abs(tfs),tout,fout,100);
    %estimate wavelet
    w=mean(abs(tfs)./spechyp);
    w=convz(w,ones(1,nf))/nf;
    spectrum=spechyp.*w(ones(length(tout),1),:);
end

```

```

if phase==1
    L1=1:length(f);L2=length(f)-1:-1:2;
    symspec=[spectrum(:,L1) spectrum(:,L2)];
    symspec2=hilbert(log(symspec')).';
    spectrum=exp(-conj(symspec2(:,L1)));
else
    spectrum=1 ./spectrum;
end

%deconvolve
if(ioperator ~= 2)
    tfs=tfs.*spectrum;
end

%inverse transform
if(ioperator == 1)
    trout=inverse_gabor(tfs,fout);
end
trout=trout(1:length(trace));
trout=balans(trout,trace);
%inverse gabor
function [trout,t]=inverse_gabor(spec,f)

[trout,t]=ifftl(sum(spec),f);

trout=trout(:);
%Gabor decon VSP-Data
[n,m]=size(sec2);
fnyq=1/(2*dt);
fmax=fnyq/2;
fwid=fnyq/20;

%Estimat Reflectivity by Gabor deconvolution
for i=1:n
    r2=gabordecon(sec4(i,:),t,.1,.01,max(t),5,0,1,1);
    r2=filtf(r2,t,[0 0],[fmax fwid]);
    r2=balans(r2,sec(i,:));
    secgabor1(i,:)=r2;
end

%Wavelet * Estimated Reflectivity = Section after Gabor
deconvolution
for i=1:n
    secgabor2=convolution(w,secgabor1(i,:),2);
    secgabor3(i,:)=secgabor2;
end

%Showing of Estimated Reflectivity
figure
formarroof(secgabor1,RS)

%Showing of Section after gabor deconvolution
figure
formarroof(secgabor3,RS)

```